Eur Biophys J (2009) 38:637–647
DOI 10.1007/s00249-009-0421-5

ORIGINAL PAPER

A nonlinear model of ionic wave propagation along microtubules

M. V. Satarić · D. I. Ilić · N. Ralević · Jack Adam Tuszynski

Received: 28 October 2008 / Revised: 27 January 2009 / Accepted: 2 February 2009 / Published online: 4 March 2009

Abstract Microtubules (MTs) are important cytoskeletal polymers engaged in a number of specific cellular activities including the traffic of organelles using motor proteins, cellular architecture and motility, cell division and a possible participation in information processing within neuronal functioning. How MTs operate and process electrical information is still largely unknown. In this paper we investigate the conditions enabling MTs to act as electrical transmission lines for ion flows along their lengths. We introduce a model in which each tubulin dimer is viewed as an electric element with a capacitive, inductive and resistive characteristics arising due to polyelectrolyte nature of MTs. Based on Kirchhoff's laws taken in the continuum limit, a nonlinear partial differential equation is derived and analyzed. We demonstrate that it can be used to describe the electrostatic potential coupled to the propagating localized ionic waves.

Keywords Microtubule · Polyelectrolyte · Nonlinear transmission line · Intrinsic electric fields · Ionic waves

M. V. Satarić · D. I. Ilić (✉) · N. Ralević
Faculty of Technical Sciences, University of Novi Sad,
Trg D. Obradovića 6, 21000 Novi Sad, Serbia
e-mail: idilic@EUnet.yu

J. A. Tuszynski
Division of Experimental Oncology, Cross Cancer Institute,
11560 University Avenue, Edmonton, AB T6G 1Z2, Canada
e-mail: jtus@phys.ualberta.ca

Introduction

The cytoskeleton is a major component of all living cells. It is made up of three different types of filamentous structures, including actin-based filaments, intermediate filaments (e.g. keratin) and tubulin based microtubules (MTs). All of them are organized into networks, which are interconnected through numerous proteins, with specific roles to play in the functioning of the cell. MTs are hollow cylinders with outer diameter of approximately 25 nm. Their lengths vary but commonly reach 5–10 μm. They are comprised of exclusively 13 parallel protofilaments in vivo. These protofilaments are strongly bound internally and are connected via weaker lateral bonds to form a sheet that is wrapped up into a tube following the nucleation process (Chrétien et al. 1995) (see Fig. 1).

Each tubulin monomer of the MT lattice has a short C-terminal helix H12 followed by a highly acidic amino acid sequence projecting out of the MT outer surface called a tubulin tail (TT). The TTs are short polypeptide sequences of 4–5 nm length when completely outstretched, protruding from the MT surface into the solution. They are essential for MT interactions with MT associated proteins and motor proteins.

Jimenez et al. (1999) determined the helicity of α (404–451) and β (394–445) tubulin C-terminal recombinant peptides with the use of NMR spectroscopy. The α-tubulin TT amino acid sequence is EEVGADSVEGEGEEEGEEY. The α-TT is 19 amino acids long and possesses ten negatively charged residues. The situation in the β-tubulin C-terminal domain is even more interesting. Jimenez et al. found a helix there, which is nine amino acids longer than in α-tubulin. This suggests an extension into the protein, supporting the possibility of a functional coil-to-helix transition at the TT zone. The β-tubulin TT helix H12 is formed by

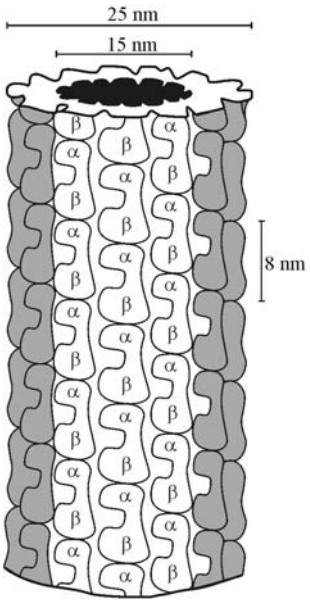

Fig. 1 Sketch of a MT cylinder with characteristic dimensions and α–β dimers clearly discerned

amino acid residues (408–431) but it seems that the reversible transition between coil and the helix comprising the last nine amino acid residues (423–431) from β-TT helix (with sequence QQYQDATAD) could either increase or decrease the length of H12, at the same time changing the β-TT length, as has been recently demonstrated using molecular dynamics simulations on human beta tubulin C-termini by Luchko et al. (2008). The corresponding residues (432–445) contain the 14 amino acids EQGEFEEEEGE DEA with nine negatively charged residues (E, A). At neutral pH the negative charge on a TT causes it to remain extended due to electrostatic repulsion within the tail (Tuszynski et al. 2005). Under more acidic conditions the negative charge of TTs is partially neutralized by associated counter-ions condensed on them. The effect is to allow the β-TTs to acquire a more compact form by folding (see Fig. 3). This is probably the largest structural effect in MTs which occurs due to change in the cell's pH. This fact will be of great importance in our model, with respect to the variable effective electrical capacitance of MTs.

The detailed charge distribution on the tubulin surface was calculated by Tuszynski et al. (2005), leading to the determination of an electrostatic potential around tubulin within a MT. It exhibits non-uniformity along the MT radius with a peak and a trough corresponding to every protofilament and the area between them, respectively. This fact plays a crucial role in our modeling of MTs as a "cable" conducting 13 parallel currents comprised of ionic flows. Keeping in mind that MTs are mostly negatively charged, especially on their outer surface, they can be referred to as polyelectrolyte polymers. This is based on the fact that numerous amino acids forming tubulin have many negatively charged residues under physiological conditions, especially those located on TTs. Since a sufficiently high surface charge density is present on the MT surface, Manning's theory (1969) can be applied to determine the conditions for the solution's positive counter-ions to "condense" on the surface of a MT. Thus, every MT should attract positive counter-ions near its surface, while negative ions of the cytosol are repelled such that a cylindrical depletion area around a MT is created. The thickness of this depleted area is defined by the so-called Bjerrum length, which is the distance from the MT surface at which the Coulomb energy of the screened surface charges equals the thermal energy:

$$\frac{e^2}{4\pi\varepsilon_0\varepsilon\ell_B} = k_B T. \tag{1.1}$$

Here, e is the charge of an electron, ε_0 the permittivity of vacuum, ε the relative permittivity of cytosol, and k_B is Boltzmann's constant. At a physiological temperature of 310 K and taking $\varepsilon = 80$, it is easy to find from Eq. 1.1 that:

$$\ell_B = 6.7 \times 10^{-10}\,\text{m}. \tag{1.2}$$

Counter-ion condensation along MTs occurs when the average distance between the intrinsic negative surface charges is smaller than ℓ_B.

The idea to examine MTs in the context of polyelectrolyte features was inspired by the experimental and theoretical results obtained earlier for actin filaments (Lin and Cantiello 1993; Tuszynski et al. 2004). From Figs. 2 and 3 it is clear that the surface of a MT filament is very rough due to the presence of TTs. We assume that the flow

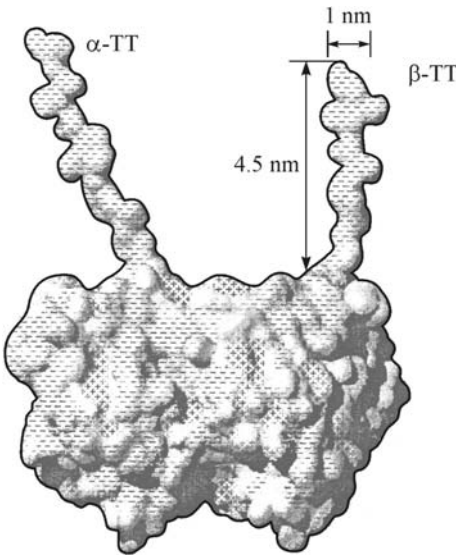

Fig. 2 Tubulin dimer charge distribution according to Tuszynski et al. (2005), with TTs and characteristic dimensions

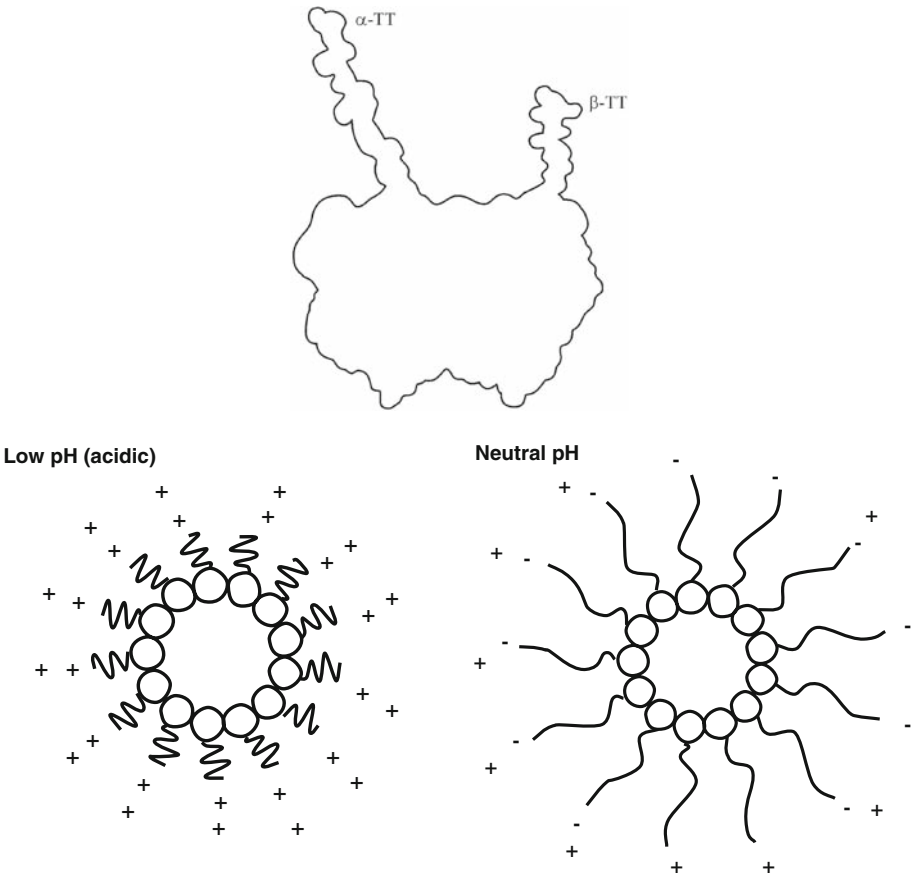

Fig. 3 *Top* shrinking of β-TT as a result of increased counterion condensation. It brings about the variable capacity of a MT as a whole. *Bottom* the conformation of TTs at (*left*) low pH and (*right*) high pH values

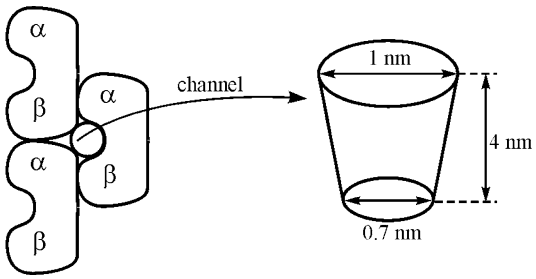

Fig. 4 Sketch of the channel connecting inner and outer surfaces of a MT

of ions along MTs, caused by the concentration gradient and by intrinsic electric fields created by the protein's charge distribution, should be mostly channeled through potential valleys (troughs) running parallel to each of the 13 protofilaments. The walls of valleys include TTs whose flexibility could significantly affect ionic current flows. In addition to the presence of TTs, it is important to note that the globular shape of tubulin dimers results in the creation of small pores representing channels that connect the inner and the outer surface of a MT (see Fig. 4).

These channels could be thought of as candidates for additional leakage of ions which would then be able to rectify currents along the depleted (Bjerrum) cylindrical layer around a MT. Recent experimental evidence (Priel et al. 2006) indicates that MTs could act as biopolymer transistors clearly amplifying input electrical signals. It is our objective in this paper to propose a model which provides an explanation of these peculiar properties of MTs and their possible role in information processing. We will follow the same theoretical approach first outlined in Tuszynski et al. (2004) for actin filaments, but it will be applied to MTs with special attention placed on their specific structural features.

The paper is organized in the following way: in Sect. "The model of MT as a nonlinear electric transmission line" we introduce the model of a MT as a nonlinear electric transmission line segmenting it into elementary rings. In Sect. "Modeling MT as nonlinear RLC transmission line" we derive and analyze a nonlinear differential equation for the local electrostatic potential coupled to the ionic wave propagating along a MT. Section "The impact of the cell's intrinsic electric fields on the dynamics of AKs in MTs" demonstrates the possible role of cell's intrinsic electric fields in the dynamics of localized ionic waves propagating along MTs. Section "Conclusion and discussion" presents a discussion and conclusions regarding this important physical mechanism in terms of the cell's electrical activity brought about by the presence of MTs and their effects on ions.

The model of MT as a nonlinear electric transmission line

We start from the fact that a MT with condensed counter-ions is separated from the rest of the ions in the bulk solution by a depleted layer which plays the role of a dielectric medium located between MTs and the bulk solution. This depleted layer provides both a resistive and capacitive component for the electrical characteristics of protofilaments that make up the MT. The injected ions are expected to flow at a radial distance from the surface of the MT with the thickness of ℓ_B. We will also estimate the inductive component of ionic waves due to 13 parallel currents and show it to be negligible compared to the other impedance components.

The estimation of elementary capacitance of a MT ring

In a continuum model we treat the MT as a polyelectrolyte represented by a volume which is bounded by a charged cylindrical surface in contact with an electrolyte (cytosol) whose dielectric constant is assumed to be time-invariant and uniform. In this case Poisson's equation is an appropriate physical description and it has the form:

$$\nabla^2 V = -\frac{\rho}{\varepsilon_0 \varepsilon}, \tag{2.1}$$

where ρ is the volume charge density at any point in the cytosol and ε is its relative dielectric constant. The charge density ρ results from the presence of counter-ions and co-ions. These are assumed to satisfy a Boltzmann distribution function. This means that in a solution containing n_s dissociated molecules of salt (for example NaCl) the number n_1 of counter-ions (Na^+) with charge $z_1 = e$ at a distance r from the MT cylinder axis is given by the expression:

$$n_1(r) = n_s \exp\left(\frac{eV}{k_B T}\right), \tag{2.2}$$

since z_1 and V have opposite signs. The number of negative (Cl^-) ions is:

$$n_2(r) = n_s \exp\left(-\frac{eV}{k_B T}\right). \tag{2.3}$$

This implies the total charge density given by:

$$\begin{aligned}\rho(r) &= n_s e\left[-\exp\left(\frac{eV}{k_B T}\right) + \exp\left(-\frac{eV}{k_B T}\right)\right] \\ &= -2n_s e \sinh\left(\frac{eV}{k_B T}\right).\end{aligned} \tag{2.4}$$

Using this result in Eq. 2.1 yields the Poisson–Boltzmann equation (PBE):

$$\nabla^2 V = \frac{2n_s e}{\varepsilon_0 \varepsilon} \sinh\left(\frac{eV}{k_B T}\right). \tag{2.5}$$

This nonlinear differential equation can be brought into a more compact form by introducing two dimensionless variables:

$$\psi = \frac{eV}{k_B T} \quad \text{and} \quad x = \frac{r}{\mathcal{D}}, \tag{2.6}$$

where the Debye length $\mathcal{D}$ is defined as:

$$\mathcal{D} = \sqrt{\frac{\varepsilon_0 \varepsilon k_B T}{2n_s e^2}}. \tag{2.7}$$

It gives:

$$\nabla^2 \psi(x) = \sinh[\psi(x)]. \tag{2.8}$$

In the Debye–Hückel approximation it is assumed that $eV \ll k_B T$ or $\psi \ll 1$, so that Eq. 2.8 can be linearized by the approximation $\sinh[\psi(x)] \approx \psi(x)$. Thus PBE in cylindrical coordinates now reads:

$$\frac{1}{x}\frac{\mathrm{d}}{\mathrm{d}x}\left(x\frac{\mathrm{d}\psi}{\mathrm{d}x}\right) = \psi \quad \text{or} \quad \frac{\mathrm{d}^2\psi}{\mathrm{d}x^2} + \frac{1}{x}\frac{\mathrm{d}\psi}{\mathrm{d}x} - \psi = 0. \tag{2.9}$$

On the surface of the MT cylinder we have: $x_0 = R/\mathcal{D}$ and $\psi_0 = eV_0/k_B T$, where R = 12.5 nm. The solution of PBE, Eq. 2.9 is a modified Bessel function of zero order denoted by $K_0(x)$, so we have:

$$\psi(x) = cK_0(x) \tag{2.10}$$

where c is the constant of integration. The above Bessel function does not oscillate and behaves asymptotically like $\exp[-x]$ as $x \to \infty$. From Eq. 2.10 one has:

$$\frac{\mathrm{d}\psi}{\mathrm{d}x} = -cK_1(x), \tag{2.11}$$

where $K_1(x)$ is the modified Bessel function of the first order. Using the relationship for the electric field:

$$E = -\frac{k_B T \mathrm{d}V}{e\mathcal{D}\ \mathrm{d}x}$$

we have:

$$-x_0\left(\frac{\mathrm{d}\psi}{\mathrm{d}x}\right)_{x=x_0} = \frac{e^2}{4\pi\varepsilon_0 \varepsilon k_B T g} = \xi; \quad g = \frac{\mathcal{L}}{N} \tag{2.12}$$

where ξ represents a scaled charge parameter of a MT, $\mathcal{L}$ is the length of a MT and Ne is the total surface charge of the same MT, Fig. 5.

Returning to the variable r, the above equations yield:

$$\psi(r) = \frac{2\xi\mathcal{D}K_0\left(\frac{r}{\mathcal{D}}\right)}{RK_1\left(\frac{r}{\mathcal{D}}\right)}. \tag{2.13}$$

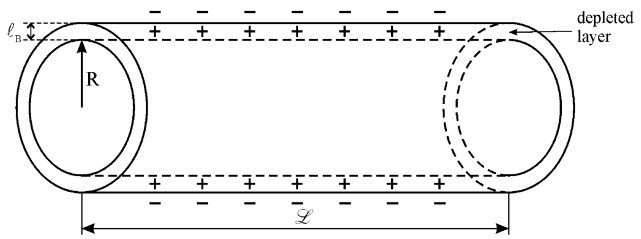

Fig. 5 MT cylinder with a depleted layer with the thickness equal to Bjerrum length ℓ_B

This equation in the case of low ionic strengths $(r/\mathcal{D} \to 0)$ behaves like $-\ln\left(\frac{r}{\mathcal{D}}\right)$, and hence we obtain the solution of PBE as:

$$V(r) = -\frac{eN}{2\pi\varepsilon_0\varepsilon\mathcal{L}}(\ln r - \ln \mathcal{D}) = -\frac{Q}{2\pi\varepsilon_0\varepsilon\mathcal{L}}\ln\left(\frac{r}{\mathcal{D}}\right). \quad (2.14)$$

The first term corresponds to the potential due to the surface charge of a MT and the second term $(\ln \mathcal{D})$ to the potential due to the counter-ions. The potential difference between the MT surface cylinder and the outer cylinder of the depleted zone at a distance ℓ_B is therefore given by:

$$\Delta V = -\frac{Q}{2\pi\varepsilon_0\varepsilon\mathcal{L}}\ln\left(1+\frac{\ell_B}{R}\right). \quad (2.15)$$

The capacitance of a MT is defined by $C = \frac{Q}{|\Delta V|}$, giving the total value for a MT:

$$C = \frac{2\pi\varepsilon_0\varepsilon\mathcal{L}}{\ln\left(1+\frac{\ell_B}{R}\right)} \quad (2.16)$$

Taking as an elementary capacitor C_0 a ring of 13 tubulin dimers with the length $\ell = 8 \times 10^{-9}$ m, and using $\varepsilon_0 = 8.85 \times 10^{-12}$ F/m, and $\varepsilon = 80$, with the above values for ℓ_B and R, we find the first part of the ring's capacitance from Eq. 2.16:

$$C_0^{(1)} = 6.8 \times 10^{-16}\,\mathrm{F} = 0.68\,\mathrm{fF}.$$

In the same way, considering an extended TT as a cylinder with length $\ell_C = 4.5$ nm and radius $R_C = 0.5$ nm we calculate an additional capacity $C_0^{(2)}$ for $n = 13 \times 2 = 26$ TTs contained in the same elementary ring composed of 13 dimers as above (see Fig. 6).

Using the same formula, Eq. 2.16, we obtain:

$$C_0^{(2)} = \frac{26 \times 3.14 \times 80 \times 8.85 \times 10^{-12} \times 4.5 \times 10^{-9}}{\ln\left(1+\frac{0.67}{0.5}\right)}\,\mathrm{F}$$
$$= 0.64 \times 10^{-15}\,\mathrm{F} = 0.64\,\mathrm{fF}.$$

Thus, treating the two contributing capacitances to be connected in parallel, the total maximal capacity of the elementary ring is found to be:

$$C_0 = C_0^{(1)} + C_0^{(2)} = 1.32 \times 10^{-15}\,\mathrm{F}. \quad (2.17)$$

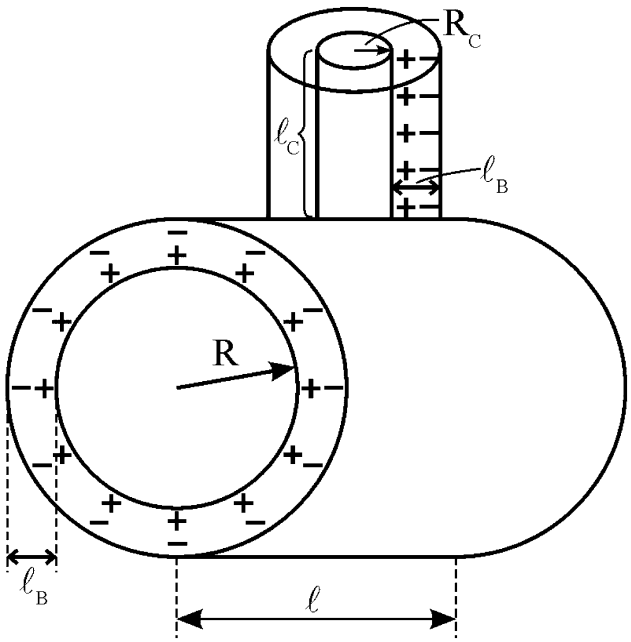

Fig. 6 Elementary ring of a MT with characteristic cylindrical capacitors and corresponding dimensions

We have already stressed that the increase of negative voltage should increase the concentration of positive counter-ions. These ions additionally condense on the surface of a MT and on TTs. This causes β-TTs to shrink diminishing their effective length ℓ_C and thus the capacity $C_0^{(2)}$. We may initially at least assume that this effect is linear with respect to the applied voltage. This observation is of crucial importance to the development of an appropriate model of MTs as nonlinear transmission lines for ionic currents.

The estimation of effective inductance of a MT ring

We start from the assumption that a current I along the MT can be conceived as a sum of 13 thin parallel wires along every protofilament (see Fig. 7).

If we calculate the resulting magnetic field in the location $R < r < R + \ell_B$, we have to add the 13 components together. Due to the radial symmetry present, we found that the total flux of the magnetic field through area $A = \ell \cdot \ell_B$ is given as follows:

$$\Phi = \frac{\mu_0 \ell I_0}{\pi}\left[\frac{3\ell_B}{R} + \frac{1}{2}\ln\left(1+\frac{\ell_B}{R_d}\right)\right],$$

where I_0 stands for the ionic current along a single protofilament and R_d is the radius of a protofilament (tubulin dimer). Using Faraday's law, we readily find the induced voltage as:

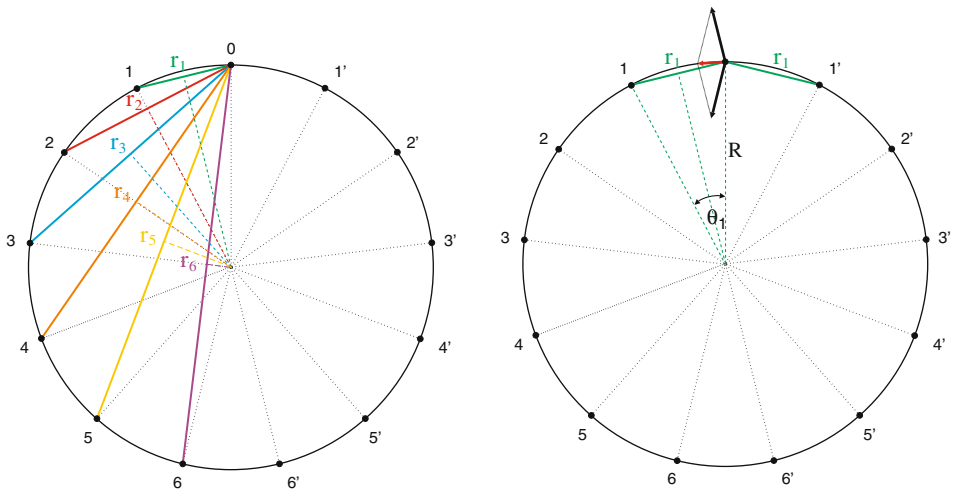

Fig. 7 The diagram for estimation of flux of magnetic field around a MT brought about by 13 currents I_0 along protofilaments

$$\mathcal{E} = -\frac{\mathrm{d}\Phi}{\mathrm{d}t} = -L\frac{\mathrm{d}I_0}{\mathrm{d}t} = -\frac{\mu_0 \ell}{\pi}\left[\frac{3\ell_\mathrm{B}}{R} + \frac{1}{2}\ln\left(1 + \frac{\ell_\mathrm{B}}{R_\mathrm{d}}\right)\right]\frac{\mathrm{d}I_0}{\mathrm{d}t},$$

which brings about the inductance of a MT ring:

$$L = \frac{\mu_0 \ell}{\pi}\left[\frac{3\ell_\mathrm{B}}{R} + \frac{1}{2}\ln\left(1 + \frac{\ell_\mathrm{B}}{R_\mathrm{d}}\right)\right]. \tag{2.18}$$

Inserting the set of parameters: $\ell = 8$ nm, $R = 12.5$ nm, $R_\mathrm{d} = 4$ nm, $\ell_\mathrm{B} = 0.67$ nm, $\mu_0 = 4\pi \times 10^{-7}$ H/m, we obtain:

$$L = 8 \times 10^{-16}\,\mathrm{H} = 0.8\,\mathrm{fH}. \tag{2.19}$$

Modeling the longitudinal and transverse resistance components

Recently published accurate measurements of individual MTs using the electro-orientational method performed in vitro by Minoura and Muto (2006) produced the value of MT conductivity:

$$\sigma = (0.15 \pm 0.01)\,\mathrm{S/m}. \tag{2.20}$$

If we now take that the resistivity within the depleted cylindrical shell around a MT with thickness ℓ_B is homogeneous, the longitudinal resistance of the elementary ring with length $\ell = 8 \times 10^{-9}$ m and area $A_1 = 2\pi R\,\ell_\mathrm{B}$ (see Fig. 8) is expected to be:

$$R_1 = \frac{1}{\sigma}\frac{\ell}{2\pi R \ell_\mathrm{B}} = \frac{8 \times 10^{-9}}{0.15 \times 2\pi \times 12.5 \times 10^{-9} \times 0.67 \times 10^{-9}}\,\Omega = 10^9\,\Omega. \tag{2.21}$$

The transversal resistance of the same ring R_2 is calculated by the same formula, but the length of each resistor is now ℓ_B and the area $A_2 = 2\pi R\,\ell$, giving:

$$R_2 = 7 \times 10^6\,\Omega. \tag{2.22}$$

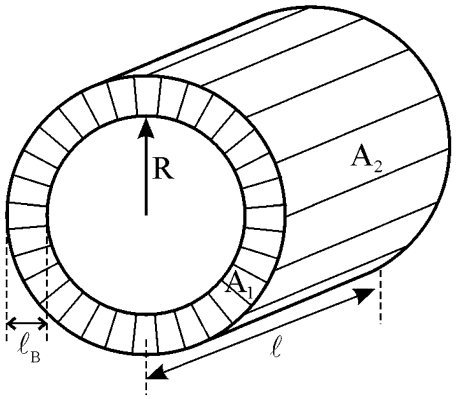

Fig. 8 Elementary ring of a MT with characteristic areas A_1 and A_2 pertaining to resistivities R_1 and R_2

Modeling MT as nonlinear RLC transmission line

On the basis of the above estimates for the resistive components of the elementary ring of a MT we are now able to develop and analyze an electrical model by applying Kirchhoff's laws to the series of elementary rings envisaged to represent coupled electrical circuits. We expect a potential difference between the MT charged surface with condensed counter-ions and ions located along the coaxial cylinder at a distance of one Bjerrum length away. These "Bjerrum ions" are responsible for the creation of 13 time-dependent currents which generate the inductance L, Eq. 2.19. In series with L one should insert a resistive component R_1, Eq. 2.21 (see Fig. 9).

In addition to the above components there is also a cylindrical capacitance C_0, Eq. 2.17 connected in series with transversal resistivity R_2, Eq. 2.22, acting between the "Bjerrum ions" and the surface of a MT. We have already

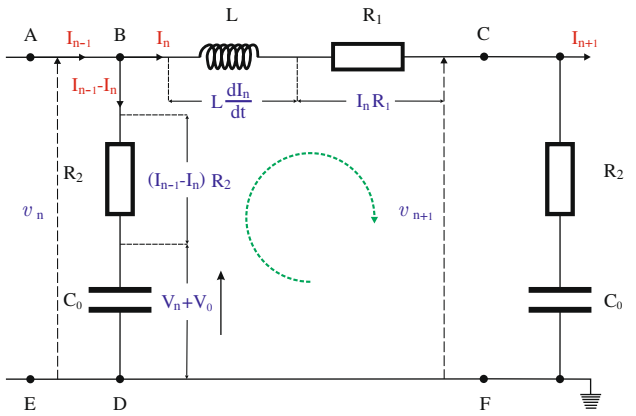

Fig. 9 An effective circuit diagram for the nth elementary ring between the doted lines

pointed out that the capacitance C_0 should change with an increasing concentration of counter-ions due to the flexibility of β-TTs. It implies that the charge on this elementary capacitor varies in a nonlinear way with voltage, much like the charge-voltage relation for a reverse-biased diode junction (Wang et al. 1999). Thus we take for the nth MT ring:

$$Q_n = C_0\left(V_n - bV_n^2\right), \tag{3.1}$$

where b is expected to be small ($bV_n \ll 1$) since the change of the area of β-TT is small compared with the outer surface of the corresponding dimer. From Kirchhoff's laws, on the basis of Fig. 9, if I_n is the current through the inductance L and the resistor R_1, and I_{n-1} is the other current flowing along AB, the current through line DB should be $I_n - I_{n-1}$. Thus for the section BC of the nth MT ring we obtain:

$$v_n - v_{n+1} = L\frac{\mathrm{d}I_n}{\mathrm{d}t} + I_nR_1, \tag{3.2}$$

where v_n and v_{n+1} are the voltages across AE and CF, respectively. Similarly, if the voltage across the variable capacitor $C_0\left(V_n - bV_n^2\right)$ is $V_n + V_0$, where V_0 is the bias voltage of the capacitor, we have:

$$v_n = R_2(I_{n-1} - I_n) + V_0 + V_n. \tag{3.3}$$

Moreover, the current through the section BD should be found as the rate of change of Q_n:

$$I_{n-1} - I_n = \frac{\mathrm{d}Q_n}{\mathrm{d}t}. \tag{3.4}$$

From Eq. 3.2 we have

$$L\frac{\mathrm{d}I_{n-1}}{\mathrm{d}t} = v_{n-1} - v_n - I_{n-1}R_1 \quad \text{and}$$
$$L\frac{\mathrm{d}I_n}{\mathrm{d}t} = v_n - v_{n+1} - I_nR_1$$

and including it in Eq. 3.4 we find

$$L\frac{\mathrm{d}^2Q_n}{\mathrm{d}t^2} = v_{n+1} + v_{n-1} - 2v_n + R_1(I_n - I_{n-1}). \tag{3.5}$$

Substituting v_{n+1}, v_n and v_{n-1} from Eqs. 3.3 to 3.5 one obtains

$$\begin{aligned} L\frac{\mathrm{d}^2}{\mathrm{d}t^2}\left[C_0\left(V_n - bV_n^2\right)\right] &= V_{n+1} + V_{n-1} - 2V_n \\ &- R_1C_0\frac{\mathrm{d}}{\mathrm{d}t}\left(V_n - bV_n^2\right) \\ &- R_2C_0\left\{2\frac{\mathrm{d}}{\mathrm{d}t}\left(V_n - bV_n^2\right) - \frac{\mathrm{d}}{\mathrm{d}t}\left(V_{n+1} - bV_{n+1}^2\right)\right. \\ &\left. - \frac{\mathrm{d}}{\mathrm{d}t}\left(V_{n-1} - bV_{n-1}^2\right)\right\}. \end{aligned} \tag{3.6}$$

Bearing in mind that voltage V_n changes gradually from ring n to its neighbors, we can safely expand V_n in a continuum approximation using a Taylor expansion in terms of a small spatial parameter ℓ (the length of a dimer):

$$\begin{aligned} V_{n\pm1} = V &\pm \ell\left(\frac{\partial V}{\partial x}\right) + \frac{\ell^2}{2!}\left(\frac{\partial^2 V}{\partial x^2}\right) \\ &\pm \frac{\ell^3}{3!}\left(\frac{\partial^3 V}{\partial x^3}\right) + \frac{\ell^4}{4!}\left(\frac{\partial^4 V}{\partial x^4}\right) \pm \cdots. \end{aligned} \tag{3.7}$$

We discarded terms on the order of ℓ^5 and ℓ^6 since $\ell^5 \sim 0.33 \times 10^{-40}$ m^5 is a very small value. The above expansion leads to the following relation:

$$V_{n+1} - 2V_n + V_{n-1} = \ell^2\left(\frac{\partial^2 V}{\partial x^2}\right) + \frac{\ell^4}{12}\left(\frac{\partial^4 V}{\partial x^4}\right). \tag{3.8}$$

Inserting Eqs. 3.7 and 3.8 into Eq. 3.6 yields:

$$\begin{aligned} LC_0\frac{\partial^2}{\partial t^2}\left(V - bV^2\right) &= \ell^2\left(\frac{\partial^2 V}{\partial x^2}\right) + \frac{\ell^4}{12}\left(\frac{\partial^4 V}{\partial x^4}\right) \\ &- R_1C_0\frac{\partial}{\partial t}\left(V - bV^2\right) + R_2C_0\frac{\partial}{\partial t}\left[\ell^2\left(\frac{\partial^2 V}{\partial x^2}\right) + \frac{\ell^4}{12}\left(\frac{\partial^4 V}{\partial x^4}\right)\right] \\ &- R_2C_0b\frac{\partial}{\partial t}\left[2\ell^2\left(\frac{\partial^2 V}{\partial x^2}\right) + 2\ell^2\left(\frac{\partial V}{\partial x}\right)^2 + \frac{\ell^4}{6}V\left(\frac{\partial^4 V}{\partial x^4}\right)\right. \\ &\left. + \frac{2}{3}\ell^4\left(\frac{\partial V}{\partial x}\right)\left(\frac{\partial^3 V}{\partial x^3}\right) + \frac{\ell^4}{2}\left(\frac{\partial^2 V}{\partial x^2}\right)^4\right]. \end{aligned} \tag{3.9}$$

The above derivation closely parallels an analogous derivation for actin filaments whose details can be found in Tuszynski et al. (2004).

Considering that the time variations of the local voltage V are small compared to the constant background voltage V_0, we can safely assume that the time derivative is of the order of the small parameter ε as well as the nonlinear

voltage terms bV^2 are of the order ε^2. Thus Eq. 3.9 can be vastly reduced by collecting only the leading terms:

$$LC_0\frac{\partial^2 V}{\partial t^2} = \ell^2\left(\frac{\partial^2 V}{\partial x^2}\right) + R_2C_0\frac{\partial}{\partial t}\left[\ell^2\left(\frac{\partial^2 V}{\partial x^2}\right)\right] - R_1C_0\frac{\partial V}{\partial t} + R_1C_0 2bV\frac{\partial V}{\partial t}. \tag{3.10}$$

Taking into account the values of L and C_0, Eqs. 2.19 and 2.17, it is clear that the factor $LC_0 \sim 10^{-30}$ s is exceedingly small and hence the second derivative term can be safely ignored. Moreover, since $R_1 \gg R_2$, the term proportional to the factor $R_2\ C_0$ can also be discarded bringing Eq. 3.10 into its final form:

$$\ell^2\frac{\partial^2 V}{\partial x^2} - R_1C_0\frac{\partial V}{\partial t} + R_1C_0 2bV\frac{\partial V}{\partial t} = 0. \tag{3.11}$$

As a first step we can linearize this equation taking $b \to 0$, which yields $b \to 0$, thus getting

$$\frac{\ell^2}{R_1C_0}\frac{\partial^2 V}{\partial x^2} = \frac{\partial V}{\partial t}. \tag{3.12}$$

This simply represents Fick's law of diffusion with a coefficient of diffusion

$$D = \frac{\ell^2}{R_1C_0} = 0.8 \times 10^{-10}\,\mathrm{m^2/s},$$

a value that, for example, falls within the experimentally observed range (Albriton et al. 1992) for calcium waves in intracellular calcium dynamics from endoplasmic reticulum.

The spatio-temporal voltage function in Eq. 3.12 follows the diffusion of ions along the MT. The solution of this equation is a well-known Gaussian wave packet that spreads with time according to:

$$V(x,t) = V_0\left(\frac{R_1C_0}{\pi\ell^2 t}\right)^{\frac{1}{2}}\exp\left\{-\left[\frac{x}{2\left(\frac{\ell^2 t}{R_1C_0}\right)^{\frac{1}{2}}}\right]^2\right\}. \tag{3.13}$$

We now analyze Eq. 3.10 by introducing a set of dimensionless variables as follows:

$$\left.\begin{aligned} &\frac{x}{\ell} = \eta; \quad \frac{t}{R_1C_0} = \tau; \quad \xi = \eta - v_0\tau \\ &V_0 = \frac{v}{v_0}; \quad v_0 = \frac{\ell}{R_1C_0}; \quad W = \frac{V}{V_0} \end{aligned}\right\} \tag{3.14}$$

Here, v is the actual propagation velocity of ionic waves while v_0 is the maximum value of the propagation velocity in a given medium.

The characteristic velocity of ionic waves is found to be

$$v_0 = \frac{8 \times 10^{-9}}{10^9 \times 1.32 \times 10^{-15}}\,(\mathrm{m/s}) = 6\,(\mathrm{mm/s}), \tag{3.15}$$

and is two orders of magnitude greater than the velocity of calcium waves in bulk cytoplasm (Wang et al. 2004). However, since $v < v_0$ ($V_0 < 1$) this appears to be a reasonably accurate estimate which is likely to correspond to the velocity of MT-guided ionic waves in vivo. In terms of the new variables in Eq. 3.14, the nonlinear partial differential equation of (3.11) now becomes an ordinary differential equation which reads:

$$\frac{\mathrm{d}^2 W}{\mathrm{d}\xi^2} + v_0\frac{\mathrm{d}W}{\mathrm{d}\xi} - 2v_0V_0bW\frac{\mathrm{d}W}{\mathrm{d}\xi} = 0. \tag{3.16}$$

Integrating it once we easily find that:

$$\frac{\mathrm{d}W}{\mathrm{d}\xi} + v_0W - v_0V_0bW^2 = c_1. \tag{3.17}$$

Interestingly, the same form of a differential equation can be found to describe the thermophoresis of biopolymers in solution (Braun and Libchaber 2004) where temperature changes linearly with distance ($T = T_0 + \alpha x$)

$$j = -D\frac{\mathrm{d}c}{\mathrm{d}x} - D_{\mathrm{T}}c(1-c)\frac{\mathrm{d}T}{\mathrm{d}x} = \mathrm{const}, \tag{3.18}$$

where $c(x)$ is the polymer concentration function, D is the diffusion coefficient, D_{T} is the thermal diffusion coefficient, and j is the steady-state current density of the polymer. This is the basis for a thermal force scenario proposing that life might have originated in pores, driven by gradients of temperature and electrical potential at hydrothermal mounds developed over submarine seepages. Moreover, if $c_1 = 0$ in Eq. 3.17, it reduces to the same mathematical form describing the logistic equation of population growth (Strogatz 1994).

In order to determine c_1 in Eq. 3.17 we impose the natural initial condition of the type

$$\frac{\mathrm{d}W}{\mathrm{d}\xi} = -A < 0, \quad \text{for} \quad W = 0.$$

Separating variables in Eq. 3.17 and factorizing it, we have

$$\int\frac{\mathrm{d}W}{W - W_1} - \int\frac{\mathrm{d}W}{W - W_2} = \alpha\xi + \ln c_2, \tag{3.19}$$

where

$$W_{1,2} = \frac{1}{2bV_0}\left[1 \pm \left(1 + 4\frac{AV_0b}{v_0}\right)^{\frac{1}{2}}\right] \quad \text{and} \quad \alpha = (W_1 - W_2)V_0v_0b > 0. \tag{3.20}$$

The integration of Eq. 3.19 with the initial conditions: $\xi = 0 \Rightarrow W = 0$, yields:

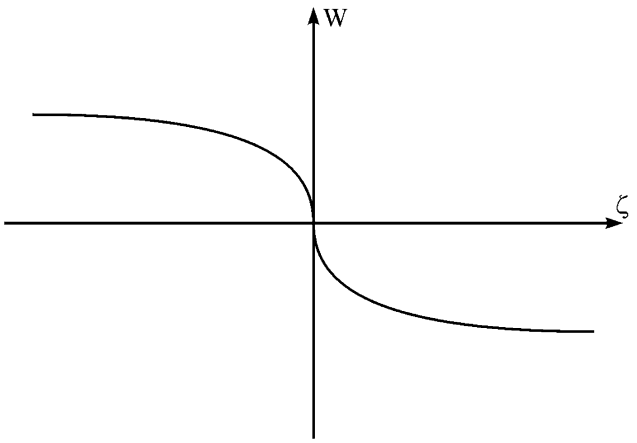

Fig. 10 The anti-kink profile of ionic potential propagating with small velocity along MT

$$W(\xi) = W_1\left[\frac{1-\exp(\alpha\xi)}{1-\frac{W_1}{W_2}\exp(\alpha\xi)}\right]. \tag{3.21}$$

Let us consider the interesting case of slow waves with velocities v_0 obeying the inequality

$$\frac{4AV_0b}{v_0} \gg 1, \tag{3.22}$$

which implies that Eq. 3.21 becomes

$$W_0(\xi) = -\left(\frac{A}{bV_0v_0}\right)^{\frac{1}{2}}\tanh(\alpha\xi), \quad \alpha = 2(AbV_0v_0)^{\frac{1}{2}}. \tag{3.23}$$

This is a symmetric anti-kink (AK) represented graphically in Fig. 10.

In order to examine Eq. 3.17 with respect to its stability we start from a slightly distorted trial solution of the form

$$W = W_0 + \delta; \quad \delta \ll W_0.$$

Inserting this trial solution into Eq. 3.17 we readily obtain

$$\frac{d^2\delta}{d\xi^2} + v_0(1-bV_0)\frac{d\delta}{d\xi} - \left(\frac{dW_0}{d\xi}\right)bV_0\delta = 0. \tag{3.24}$$

Since the inequalities

$$bV_0 \ll 1; \quad \frac{dW_0}{d\xi} < 0$$

always hold, this clearly indicates that the AK of Eq. 3.23 represents a robust stable front of propagating ionic wave as shown in Fig. 10.

The impact of the cell's intrinsic electric fields on the dynamics of AKs in MTs

Satarić et al. (1993, 2007) and Satarić and Tuszynski (2003, 2005) developed the ferroelectric model of MTs with oppositely charged ends as giant dipoles arising as a consequence of the fact that every tubulin dimer possesses an intrinsic electric dipole (see Fig. 11) that becomes compensated by the dipoles of its neighbors only partially.

These ferroelectric features of MTs lead to the conclusion that every MT has an intrinsic, almost constant, electric field E whose magnitude depends on the environmental pH conditions and the MT length. This field gives rise to an additional potential V_{int}. In this context the dimensionless Eq. 3.16 cab be analyzed numerically by taking into account V_{int}.

If we judiciously choose the set of parameters:

$$v_0 = 0.1, \quad v_0bV_0 = 0.05, \quad \frac{V_{int}}{V_0} = 0.4,$$

we have the resultant equation in the form

$$\frac{d^2W}{d\xi^2} + 0.1\frac{dW}{d\xi} - 0.05W\frac{dW}{d\xi} + 0.1 = 0. \tag{4.1}$$

Taking the initial conditions as

$$\frac{dW}{d\xi}(0) = -0.5, \quad W(0) = 0$$

we calculate the trajectory for the center of the AK as a function of the dimensionless time represented graphically in Fig. 12.

This figure shows that the AK is initially driven by acceleration and after $\tau = 50(t \sim 0.5\,\mu s)$ it attains a constant terminal velocity $V_0 = 0.1$ ($v = 0.1 \cdot v_0 \approx 600$ μm/s) which is reasonably close to the experimentally determined values for waves of Ca^{2+} ions.

We further assume that certain intrinsic alternating electric fields (IAEF) can be elicited in the cell's compartments. It was already suggested earlier that such fields can originate from the oriented (vicinal) water molecules which form an electric dipole field occurring on either side

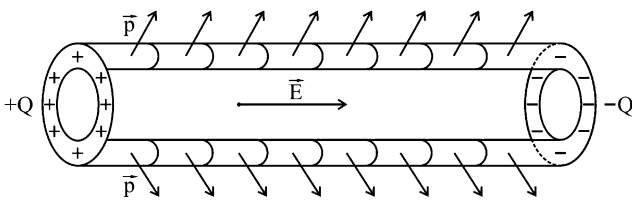

Fig. 11 Ferroelectric features of a MT. The charged tips bring about a constant intrinsic electric field E

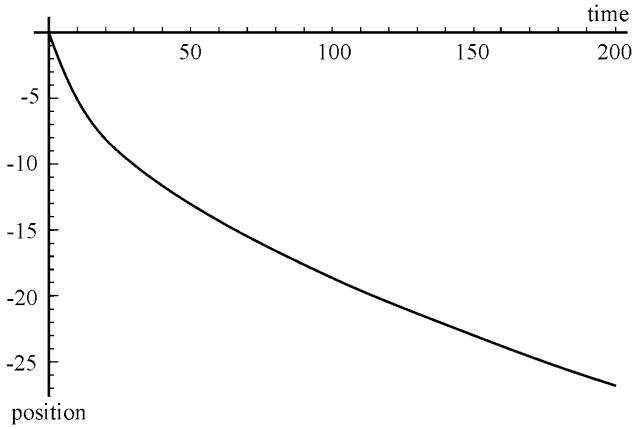

Fig. 12 The trajectory of the center of AK under the action of constant intrinsic electric field, Eq. 4.1

of the cell membrane. Del Giudice et al. (1988) have proposed that electromagnetic fields arising from the coherent oscillations of the above-mentioned water molecules represent signals comparable in size with the dimensions of the cell's MTs. It is potentially of major significance that MTs themselves may be a source of oscillating electric fields in living cells as discussed by Pokorny et al. (2005). We can safely assume that the associated dimensionless driving force has a wavelength greater than the average MT length and it harmonically depends on the dimensionless time τ as follows

$$V_{\mathrm{WF}}(\tau) = A_0 \cos(\Omega\tau + \varphi_0), \tag{4.2}$$

where A_0 is the amplitude, Ω is the frequency and φ_0 is the initial phase of the potential of the water field (WF). Using the same parameters for the homogeneous part of Eq. 4.1 as those used before, and taking $A_0 = 0.5$, $\Omega = 0.5$ and $\varphi_0 = 0$, we have

$$\frac{\mathrm{d}^2 W}{\mathrm{d}\xi^2} + 0.1\frac{\mathrm{d}W}{\mathrm{d}\xi} - 0.05W\frac{\mathrm{d}W}{\mathrm{d}\xi} + 0.1 = 0.5\cos(0.5\tau). \tag{4.3}$$

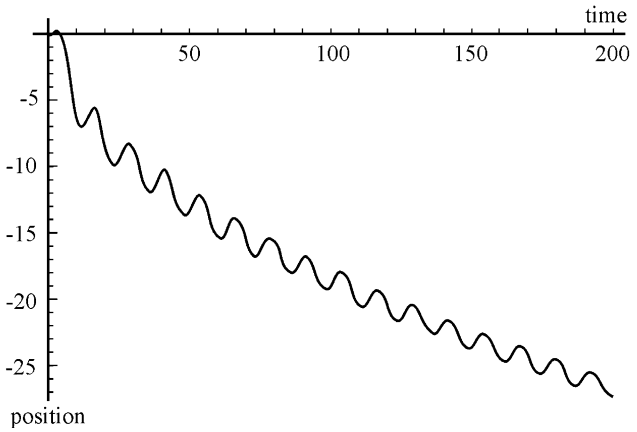

Fig. 13 The trajectory of the center of AK subjected to constant and harmonically changeable intrinsic electric fields, Eq. 4.3

A numerical solution of the above equation produces a trajectory of the corresponding AK as shown in Fig. 13.

We have again found similar characteristics of the unidirectional AK motion with the same average velocity but now superimposed with harmonic oscillations around the center of the AK.

Conclusion and discussion

A new model for ionic currents along MTs has been presented in this paper with a strong emphasis on the concept of a MT as a polyelectrolyte. The background for the model is the molecular structure and geometry of a MT and its interaction with solvent ions. In this context the MT cylinder with brush-like TTs surrounded by ions from cytosol is represented as an electrical transmission line with R, C and L elements whose values have been estimated using the available experimental data and known geometry. The important feature of the nonlinearity of MT capacitance has arisen naturally from the structure of β-TTs. As a result, the nonlinear second order differential equation for the electric potential propagating along the MT was evaluated. The traveling wave solution of this equation, Eq. 3.16, is a localized front profile of the AK type. This front resembles a so-called "nano-tsunami" and it propagates with a velocity which has been estimated to be reasonably close to the experimental findings, for example for waves of Ca^{2+} ions elicited by endosome reticulum compartments. These AKs appear to be stable and robust against perturbations. The remaining part of the paper has been dedicated to the possible impact of the cell's endogenous (intrinsic) electric fields on the dynamics of ionic AKs. It appears that the velocity and direction of propagation of an AK could be tuned by changing the parameters of the above-mentioned fields (i.e. their amplitude, frequency and phase). It is our hope that the model developed here will provide a better insight into the still unknown roles of MTs in the cell's information processing capabilities.

Acknowledgments The authors from Faculty of Technical Sciences are grateful for grants 141018A and 23036 provided by the Government of Serbia. JAT gratefully acknowledges funding for this project from NSERC, Alberta Cancer Foundation, the Allard Foundation and Alberta's Advanced Education and Technology.

References

Albriton NL, Meyer T, Stryer L (1992) Range of messenger activation of calcium ions and IP3. Science 258:1812–1815

Braun D, Libchaber A (2004) Thermal force approach to molecular evolution. Phys Biol 1:P1–P8

Chrétien D, Fuller SD, Karsenti E (1995) Structure of growing microtubule ends: two-dimensional sheets close into tubes at variable rates. JCB 129(5):1311–1328

Del Giudice, Preparata G, Vitiello G (1988) Water as a free electric dipole laser. Phys Rev Lett 61:1085–1088

Jimenez MA, Evangelio JA, Aranda C, Lopez-Brauet A et al (1999) Helicity of alpha (404–451) and beta (394–445) tubulin C-terminal recombinant peptides. Protein Sci 8:788–799

Lin EC, Cantiello HF (1993) A novel method to study the electrodynamic behavior of actin filaments. Evidence for cable-like properties of actin. Biophys J 65(4):1371–1378

Luchko L, Huzil JT, Stepanova M, Tuszynski JA (2008) Conformational analysis of the carboxy-terminal tails of human beta tubulin isotypes. Biophys J 94:1971–1982

Manning GS (1969) Limiting laws and counterion condensation in polyelectrolyte solutions I. Colligative properties. J Chem Phys 51:924–933

Minoura I, Muto E (2006) Dielectric measurement of individual microtubules using the electroorientation method. Biophys J 90:3739–3748

Pokorný J, Hašek J, Jelínek F (2005) Electromagnetic field of microtubules: effects of transfer of mass particles and electrons. J Biol Phys 31:501–514

Priel A, Ramos AJ, Tuszynski JA, Cantiello HF (2006) A biopolymer transistor: electrical amplification by microtubules. Biophys J 90:4639–4643

Satarić MV, Tuszynski JA (2003) Relationship between the nonlinear ferroelectric and liquid crystal models for microtubules. Phys Rev E 67:011901–011912

Satarić MV, Tuszynski JA (2005) Nonlinear dynamics of microtubules and its biophysical implications. J Biol Phys 31:487–496

Satarić MV, Tuszynski JA, Žakula RB (1993) Kinklike excitations as an energy-transfer mechanism in microtubules. Phys Rev E 48:589–597

Satarić MV, Budinski-Petković Lj, Lončarević I (2007) Microtubules as active tracks for bi-directional cellular traffic of motor proteins. IJMPB 21(32):5387–5398

Strogatz SH (1994) Nonlinear dynamics and chaos. Addison-Wesley, Reading

Tuszynski JA, Portet S, Dixon JM, Luxford C, Cantiello HF (2004) Ionic wave propagation along actin filaments. Biophys J 86:1890–1903

Tuszynski JA, Brown JA, Crawford E, Carpenter EJ, Nip MLA, Dixon JM, Satarić MV (2005) Molecular dynamics simulations of tubulin structure and calculations of electrostatic properties of microtubules. Math Comput Model 41:1055–1070

Wang BG, Zhao XA, Wang J, Guo H (1999) Nonlinear quantum capacitance. Appl Phys Lett 74:2887–2999

Wang K, Rappel W-J, Levine H (2004) Cooperativity can reduce stochasticity in intracellular calcium dynamics. Phys Biol 1:27–34